Formation of *mos* RNA granules in the zebrafish oocyte that differ from *cyclin B1* RNA granules in distribution, density and regulation

Mayu Horie[a] and Tomoya Kotani[a,b,*]

[a]Biosystems Science Course, Graduate School of Life Science, Hokkaido University, Sapporo 060-0810, Japan

[b]Department of Biological Sciences, Faculty of Science, Hokkaido University, Sapporo 060-0810, Japan

*Corresponding author.
Tomoya Kotani,
Department of Biological Sciences, Faculty of Science, Hokkaido University,
North 10 West 8, Sapporo, Hokkaido 060-0810, Japan
Tel.: +81-11-706-4455
Fax.: +81-11-706-4455
E-mail: tkotani@sci.hokudai.ac.jp

Running title: Formation of distinct RNA granules in zebrafish oocytes

Abstract

Many translationally repressed mRNAs are deposited in the oocyte cytoplasm for progression of the meiotic cell cycle and early development. *mos* and *cyclin B1* mRNAs encode proteins promoting oocyte meiosis, and translational control of these mRNAs is important for normal progression of meiotic cell division. We previously demonstrated that *cyclin B1* mRNA forms RNA granules in the zebrafish and mouse oocyte cytoplasm and that the formation of RNA granules is crucial for regulating the timing of translational activation of the mRNA. However, whether the granule formation is specific to *cyclin B1* mRNA remains unknown. In this study, we found that zebrafish *mos* mRNA forms granules distinct from those of *cyclin B1* mRNA. Fluorescent in situ hybridization analysis showed that *cyclin B1* RNA granules were assembled in dense clusters, while *mos* RNA granules were distributed diffusely in the animal polar cytoplasm. Sucrose density gradient ultracentrifugation analysis showed that the density of *mos* RNA granules was partly lower than that of *cyclin B1* mRNA. Similar to *cyclin B1* RNA granules, *mos* RNA granules were disassembled after initiation of oocyte maturation at the timing at which the poly(A) tail was elongated. However, while almost all of the granules of *cyclin B1* were disassembled simultaneously, a fraction of *mos* RNA granules firstly disappeared and then a large part of them was disassembled. In addition, while *cyclin B1* RNA granules were disassembled in a manner dependent on actin filament depolymerization, certain fractions of *mos* RNA granules were disassembled independently of actin filaments. These results suggest that cytoplasmic regulation of translationally repressed mRNAs by formation of different RNA granules is a key mechanism for translational control of distinct mRNAs in the oocyte.

Key words: vertebrate, mRNA localization, oocyte maturation, translational control

1. Introduction

Vertebrate oocytes arearrested at prophase I of the meiotic cell cycle and accumulate translationally repressed mRNAs in order to promote oocyte meiosis and development (de Moor et al., 2005; Masui and Clarke, 1979; Mendez and Richter, 2001). These oocytes are unable to be fertilized and are called immature oocytes. Full-grown oocytes in this stage resume meiotic cell division in response to specific signals such as hormones in species-specific breeding seasons (Masui and Clarke, 1979). After resumption of meiosis, oocytes of many vertebrate species are arrested again at meiotic metaphase II. This process is termed oocyte maturation and is necessary for oocytes to acquire fertility. Since transcription becomes quiescent after induction of oocyte maturation, most processes that occur during oocyte maturation and early development are driven by synthesis of proteins from stored mRNAs in oocytes.

Maturation/M-phase-promoting factor (MPF) is one of the important and universal factors for driving the progression of meiotic cell division (Masui and Clarke, 1979; Nurse, 1990). MPF consists of a catalytic subunit of Cdc2 and a regulatory subunit of Cyclin B. In fish and amphibians except *Xenopus*, Cyclin B is absent in immature oocytes (Ihara et al., 1998; Kondo et al., 1997; Kotani and Yamashita, 2002; Tanaka and Yamashita, 1995). Therefore, synthesis of Cyclin B from mRNA that has accumulated in the oocyte cytoplasm is prerequisite for the formation and subsequent activation of MPF, which induces germinal vesicle breakdown (GVBD), chromosome condensation and spindle formation. Although synthesis of Cyclin B is not necessary for GVBD in *Xenopus* and mouse oocytes, newly synthesized Cyclin B is required for meiotic metaphase I to II transition that occurs without DNA replication (Hochegger et al., 2001; Ledan et al., 2001).

Mos protein plays crucial roles during the progression of meiotic cell division and in metaphase II arrest as a component of the cytostatic factor (CSF). Mos is synthesized after induction of oocyte maturation and immediately activates the mitogen-activated protein kinase (MAPK) pathway. Mos-deficient oocytes and oocytes treated with MAPK inhibitors undergo GVBD but fail to form normal spindles in fish, frogs and mice (Araki et al., 1996; Choi et al., 1996; Dupre et al., 2002; Fisher et al., 1999; Gross et al., 2000; Kajiura-Kobayashi et al., 2000; Kotani and Yamashita, 2002; Verlhac et al., 1996). These oocytes form nuclei in meiotic metaphase I to II transition and fail to arrest at metaphase II due to a decrease in the MPF activity after entry into the second

meiotic division.

In addition to the synthesis of Cyclin B and Mos from stored mRNAs, temporally ordered translation of these mRNAs after induction of oocyte maturation is also important for normal progression of meiotic cell division. For instance, it was shown that precocious activation of MPF caused defects in spindle formation and chromosome segregation in frog and mouse oocytes (Davydenko et al., 2013; Kotani and Yamashita, 2002). In addition, the timing of activation of the MAPK pathway prior to the activation of MPF is important for chromosome condensation and microtubule organization to form a normal spindle apparatus in frog oocytes (Kotani and Yamashita, 2002).

One of the mechanisms promoting translational activation of the dormant mRNAs with a short poly(A) tail is cytoplasmic polyadenylation of the mRNAs (McGrew et al., 1989; Sheets et al., 1994; Vassalli et al., 1989). The cytoplasmic polyadenylation element (CPE) located on the 3' untranslated region (3'UTR) of certain numbers of mRNAs including *mos* and *cyclin B1* and CPE-binding protein CPEB function in both repression and direction of the cytoplasmic polyadenylation (Barkoff et al., 2000; de Moor and Richter, 1999; Gebauer et al., 1994; Tay et al., 2000). Pumilio-binding element (PBE) located on the 3'UTR of *cyclin B1* mRNA and its binding protein Pumilio are involved in translational activation at the timing that is specific to *cyclin B1* (Nakahata et al., 2001; Nakahata et al., 2003; Ota et al., 2011; Pique et al., 2008). Musashi-binding element (MBE) located on the 3'UTR of *Xenopus mos* mRNA and its binding protein Musashi direct translational activation in an early period after induction of oocyte maturation (Charlesworth et al., 2002; Charlesworth et al., 2006). These studies demonstrated the importance of particular *cis*-acting elements and *trans*-acting factors that regulate the state of poly(A) length. However, the precise cytoplasmic regulation of dormant mRNAs in oocytes remains to be investigated.

We previously reported the identification of *cyclin B1* RNA granules in the zebrafish and mouse oocyte cytoplasm (Kotani et al., 2013). These RNA granules disassembled shortly after induction of maturation at the timing at which poly(A) tails are elongated. The disruption and stabilization of RNA granules induced acceleration and prevention of translational activation of the mRNA, respectively. Therefore, the assembly and dissociation of *cyclin B1* RNA granules appear to direct translational repression and activation of the mRNA. However, whether this regulation is specific to *cyclin B1* mRNA remains unknown.

In this study, we found that the zebrafish *mos* mRNA forms RNA granules within the animal polar cytoplasm of immature oocytes as in the case of the *cyclin B1* mRNA. The *mos* RNA granules were, however, different from those of *cyclin B1* in distribution and density. In addition, the *mos* RNA granules gradually disassembled at the timing of their polyadenylation after induction of oocyte maturation, in contrast to rapid disassembly of *cyclin B1* RNA granules. Our results indicate the presence of distinct cytoplasmic regulation of dormant mRNAs as formation of different granules and suggest the importance of formation and disassembly of RNA granules in temporal and spatial control of mRNA translation in oocytes.

2. Materials and Methods

2.1. Preparation of ovaries

All animal experiments in this study were approved by the Committee on Animal Experimentation, Hokkaido University. Zebrafish ovaries were dissected from adult females in zebrafish Ringer's solution (116 mM NaCl, 2.9 mM KCl, 1.8 mM $CaCl_2$, and 5 mM HEPES; pH 7.2). For in situ hybridization analysis, zebrafish ovaries were fixed with 4% paraformaldehyde in PBS (4% PFA/PBS) overnight at 4˚C. For sucrose density gradient ultracentrifugation analysis, zebrafish ovaries were homogenized with an equal volume of ice-cold extraction buffer (EB: 100 mM β-glycerophosphate, 20 mM HEPES, 15 mM $MgCl_2$, 5 mM EGTA, 1 mM dithiothreitol, 100 μM (*p*-amidinophenyl)methanesulfonyl fluoride, 3 μg/ml leupeptin; pH 7.5) containing 100 units/ml RNasin Plus RNase Inhibitor (Promega). After centrifugation at 5,000 rpm for 5 min at 4˚C, the supernatant was collected and used for ultracentrifugation.

2.2. Section *in situ* hybridization

Section *in situ* hybridization was performed according to the procedure reported previously (Kondo et al., 2001). Fluorescent in situ hybridization (FISH) with the tyramide signal amplification (TSA) Plus DNP system (PerkinElmer) was performed according to the procedure reported previously (Kotani et al., 2013). Briefly, fixed ovaries and oocytes were dehydrated, embedded in paraffin, and cut into 10-μm-thick sections. A digoxigenin (DIG)-labeled antisense RNA probe for the full length, 5' half

(1-609 bases) or 3’ half (613-1168 bases) of *mos* was used for detection of the *mos* gene transcript. No signal was detected with sense probes. After hybridization and washing, samples were incubated with anti-DIG-horseradish peroxidase (HRP) antibody (Roche) (1:500 dilution) for 30 min. The reaction with tyramide-dinitrophenyl (DNP) was performed according to the manufacturer’s instructions. The samples were then incubated overnight with anti-DNP-Alexa 488 antibody (Molecular Probes) (1:500 dilution). To detect nuclei, the samples were incubated with 10 µg/ml Hoechst 33258 for 10 min. After being mounted with Prolong Antifade Kit (Molecular probes), the samples were observed under an LSM5LIVE confocal microscope (Carl Zeiss). The number of *mos* and *cyclin B1* RNA granules was quantified using ImageJ software, which enables detection of granules according to size (larger than 0.2 µm) and intensity at the center of granules.

Double *in situ* hybridization of *mos* and *cyclin B1* transcripts was performed as follows. A fluorescein-labeled antisense RNA probe for *cyclin B1* was used for detection of the *cyclin B1* gene transcript. Ten-µm-thick sections of zebrafish ovaries were hybridized with a mixture of *mos* and *cyclin B1* antisense RNA probes. After detection of the DIG-labeled antisense *mos* RNA probe, the samples were incubated with 1% H_2O_2 in PBS for 1 h for inactivating HRP. After washing with PBS, the samples were incubated with anti-Fluorescein-HRP antibody (Roche) (1:200 dilution) for 30 min. The reaction with tyramide-Cy3 was performed according to the manufacturer’s instructions. A fluorescein-labeled antisense RNA probe for *mos* and a DIG-labeled antisense RNA probe for *cyclin B1* were also used for double *in situ* hybridization. Detection of the DIG- and fluorescein-labeled RNA probes was performed as described above. After staining with Hoechst 33258, the samples were mounted and observed under the LSM5LIVE confocal microscope.

2.3. Sucrose density gradient ultracentrifugation

Sucrose density gradient ultracentrifugation was performed according to the procedure reported previously (Takahashi et al., 2014) with modifications. Briefly, 500 µl of ovary extracts was loaded onto 4 ml of 5%-65% sucrose gradient prepared in a Hitachi centrifuge tube (Hitachi Koki) with a dialysis buffer (100 mM β-glycerophosphate, 20 mM HEPES, 15 mM $MgCl_2$, 5 mM EGTA; pH 7.5) using Gradient Master (BioComp Instruments). After centrifugation at 35,000 rpm in an

S52ST rotor (Hitachi) for 5 h at 4˚C, the sucrose gradient was collected in 10 equal fractions from the bottom of the tube. Distribution of proteins in the sucrose gradient was analyzed by CBB staining and immunoblotting after SDS-PAGE. The amounts of *mos* and *cyclin B1* mRNAs were analyzed by quantitative RT-PCR after extraction of total RNA from distinct fractions with Trizol reagent (Ambion). Full lengths of *mos* and *cylin B1* RNAs were synthesized using the Riboprobe System-T3 kit (Promega) according to the manufacturer's instructions. One μg of the synthesized RNAs was loaded, centrifuged, and fractioned. The amounts of RNAs in distinct fractions were analyzed by quantitative RT-PCR. Forty μg of fluorescein dextran (500,000 molecular weight, Molecular probe) was loaded, centrifuged, and fractioned. The intensity of fluorescein was measured by using Fluorescence Spectrophotometer F-2500 (Hitachi). To confirm that *mos* and *cyclin B1* mRNAs in heavy fractions were not bound to polysomes, the oocytes were incubated with 40 μg/ml puromycin in zebrafish Ringer's solution for 20 min. The oocytes were homogenized with EB and centrifuged at 5,000 rpm for 5min at 4˚C. The supernatant was loaded onto the sucrose gradient containing 40 μg/ml puromycin, centrifuged, and fractioned.

2.4. Immunoblotting

The fractions from sucrose gradient ultracentrifugation were separated by SDS-PAGE, blotted onto an Immobilon membrane, and probed with anti-human RPL11 polyclonal antibody (Abcam).

2.5. Induction of oocyte maturation

Zebrafish oocytes were manually isolated from ovaries with forceps under a dissecting microscope. Oocyte maturation was induced by treatment with 1 μg/ml of 17α,20β-dihydroxy-4-pregnen-3-one, an MIH in fish. For FISH analysis, oocytes were fixed with 4% PFA/PBS at intervals of 30 min after MIH stimulation. For quantification of the amount of *mos* and *cyclin B1* mRNAs, full-grown immature oocytes and oocytes 3 h after MIH stimulation (matured oocytes) were extracted with Trizol reagent and the total RNAs were used for quantitative RT-PCR.

2.6. Quantitative RT-PCR

Total RNA extracted from distinct fractions of density gradient ultracentrifugation

and 50 immature or matured oocytes was used for cDNA synthesis using the Super Script III First Strand Synthesis System (Invitrogen). The amount of *mos* and *cyclin B1* mRNAs was quantified by using a real-time PCR system with SYBR green PCR Master Mix (Applied Biosystems) according to the manufacturer's instructions. The *mos* and *cyclin B1* transcripts were amplified with the cDNA and primer sets specific to *mos*, z*mos*-qPCR-f (5'-CGT AAT GGA GTT CGC AGG CAA TA-3') and z*mos*-qPCR-r (5'-TCT GAC AAC AAG ACA TTG GCT GG-3'), and *cyclin B1*, z*cyclin B1*-qPCR-f (5'-GAC AGG CTT TGA AGA AGA AGG AGG-3') and z*cyclin B1*-qPCR-r (5'-GGA AGG CTC AGA CAC AAC CTT AA-3'). The signals obtained with distinct primer sets were normalized by standard curves obtained with plasmid DNAs encoding the *mos* or *cyclin B1* gene.

2.7. Poly(A) test (PAT) assay

RNA ligation-coupled RT-PCR was performed according to the procedure reported previously (Charlesworth et al., 2004; Yasuda et al., 2010). Two µg of total RNA extracted from pools of 15 zebrafish oocytes was ligated to 0.4 µg of P1 anchor primer (5'-P-GGT CAC CTT GAT CTG AAG C-NH_2-3') in a 10-µl reaction using T4 RNA ligase (New England Biolabs) for 30 min at 37˚C. The ligase was inactivated for 5 min at 92˚C. Half of the RNA ligation reaction was used in a 25-µl reverse transcription reaction using Superscript III First Strand Synthesis System with a P1' primer (5'-GCT TCA GAT CAA GGT CTT TTT TTT-3'). Four µl of the cDNA was used for the 1st PCR with the P1' primer and a z*mos*-PAT-f1 primer (5'-TAT AAC CTG CGC CCT TTG ACC AGC-3') or z*cyclin B1*-PAT-f1 primer (5'-GAG GGC CTT TCT AAG CAT CTG GCT GTG-3') for 17 cycles. Two µl of the 1st PCR reaction was used for the 2nd PCR with the P1' primer and a z*mos*-PAT-f2 primer (5'-ATA TTG TAA ATG TTC GTG TTT TTG TTT TAT TGT GAA GC-3') or z*cyclin B1*-3'UTR-f primer (5'-TAC GGA TTT CTT CAC TGC CAT G-3') for 35 cycles. The PCR product was resolved on a 2% TAE gel. We confirmed that the increase in PCR product length was due to elongation of the poly(A) tails by cloning the 2nd PCR products and sequencing them.

2.8. Jasplakinolide treatment

To stabilize actin filaments, oocytes were treated with 5 µM jasplakinolide (Calbiochem), which prevents depolymerization of actin filaments in oocytes treated

with MIH (Kotani et al., 2013), for 3 h. Jasplakinolide was dissolved in dimethyl sulfoxide (DMSO) as stocks and diluted in Ringer's solution before use. As a control, oocytes were treated with 0.5% DMSO.

3. Results

3.1. Formation of *mos* RNA granules in immature oocytes

Localization of *mos* mRNA in oocytes was first examined by *in situ* hybridization of zebrafish ovaries using the full length of the antisense *mos* RNA probe. *mos* mRNA was detected in the animal polar cytoplasm of immature oocytes beneath the micropyle, a structure through which a sperm enters into the oocyte cytoplasm (Fig. 1A), consistent with results reported previously (Suzuki et al., 2009). The distribution of *mos* mRNA was then analyzed by fluorescent *in situ* hybridization (FISH) with the tyramide signal amplification (TSA) system. Bright, but small, particles were observed diffusely throughout the animal polar cytoplasm beneath the micropyle (Fig. 1B and C). Similar results were obtained by using antisense *mos* RNA probes consisting of the 5' half (1-609 bases) and 3' half (613-1168 bases) of *mos* sequences (Fig.1 D, E and F). Therefore, the diffused signals do not result from low hybridization efficiency of the full-length probe. Taken together, these results indicate the presence of *mos* RNA granules in oocytes.

3.2. Formation of distinct RNA granules in the oocyte cytoplasm

The detection of *mos* RNA granules in the animal polar cytoplasm of immature oocytes suggested that the localization and translation of *mos* and *cyclin B1* mRNAs are regulated by formation of the same granules. To assess this possibility, we simultaneously detected *mos* and *cyclin B1* mRNAs by FISH analysis using DIG-labeled antisense *mos* and fluorescein-labeled *cyclin B1* RNA probes. Interestingly, *mos* and *cyclin B1* mRNAs were distributed in similar regions of the animal polar cytoplasm (Fig. 2A, B and C) by forming distinct RNA granules (Fig. 2D, E and F). The *mos* RNA granules rarely overlapped with the *cyclin B1* RNA granules (4.9%, n = 638). The distributions of these RNA granules were also different. The *mos* RNA granules were diffusely distributed in the animal polar cytoplasm (Fig. 2D; Figs. 5 and 7), while the

cyclin B1 RNA granules were densely distributed and appear to form clusters (Fig. 2E; Figs. 5 and 7) (Kotani et al., 2013). Similar results were obtained by using fluorescein-labeled antisense *mos* and DIG-labeled antisense *cyclin B1* RNA probes (Fig. 2G, H and I). Therefore, the differences in FISH signals do not result from different sensitivities in the detection of DIG- and fluorescein-labeled RNA probes. Quantitative RT-PCR using RNAs purified from immature oocytes showed that the amount of *cyclin B1* mRNA was 3-fold larger than that of *mos* mRNA (3.0 ± 0.3, n = 5), suggesting that the differences in the number, distribution and diameter of RNA granules were, at least in part, due to the differences in the amounts of mRNAs.

3.3. Difference in densities of *mos* and *cyclin B1* RNA granules

We then examined the densities of *mos* and *cyclin B1* RNA granules by sucrose density gradient ultracentrifugation. The ovary extracts were dissected into 10 fractions according to the sucrose density gradient from 5% (fraction 1) to 65% (fraction 10) after centrifugation. In the sucrose gradient, most proteins were distributed from fractions 1 to 6 (Fig. 3A, top). Rpl11, one of ribosomal proteins, was distributed from fractions 5 to 10 and the amounts in fractions 8, 9 and 10 were larger than those in fractions 5, 6 and 7 (Fig. 3A, bottom). Dextran of 500,000 molecular weight was concentrated in fractions 2 and 3 (Fig. 3B). Quantitative RT-PCR using purified RNAs of distinct fractions showed that the *mos* and *cyclin B1* mRNAs were broadly distributed from fractions 5 to 10 in slightly different manners (Fig. 3C). First, the percentage of *mos* mRNA in fraction 10 (3.8 ± 1.9%) was statistically smaller than that of *cyclin B1* mRNA (6.7 ± 0.7%, $P < 0.05$, Student's *t*-test). Second, the percentage of *mos* mRNA in fraction 6 (21.5 ± 1.8%) was larger than that in fraction 7 (16.3 ± 3.6 %, $P < 0.05$, Student's *t*-test), while no statistical difference was shown in the percentages of *cyclin B1* mRNA from fractions 5 to 9. Treatment with puromycin, which disrupts polysomes, significantly reduced Rpl11 in fractions 8, 9 and 10 (Fig. 3E). In contrast, puromycin treatment did not affect the distribution of *mos* and *cyclin B1* mRNAs (Fig. 3F). Therefore, the *mos* and *cyclin B1* mRNA in heavy fractions were not related to polysomes.

We then analyzed the distributions of *in vitro* synthesized *mos* and *cyclin B1* RNAs after centrifugation. The *mos* and *cyclin B1* RNAs showed similar distribution patterns, i.e., most of them were concentrated in fractions 3, 4 and 5 (Fig. 3D). Apparent amounts of *mos* and *cyclin B1* RNAs were also detected in fractions 7, 8 and 9 (Fig. 3D),

suggesting oligomer formation of each RNA during synthesis and centrifugation. Taken together, the results of sucrose density gradient ultracentrifugation indicate that *mos* and *cyclin B1* mRNAs form large complexes in the oocyte cytoplasm and suggested that the molecular weight of *mos* RNA granules is partly smaller than that of *cyclin B1* RNA granules.

3.4. Disappearance of *mos* RNA granules during oocyte maturation

The relationship between RNA granule formation and translational control of the *mos* mRNA was first examined by FISH analysis of immature and mature oocytes. *mos* RNA granules were observed in the cytoplasm of immature oocytes but not in that of mature oocytes (Fig. 4A and B). The amount of *mos* mRNA was maintained in mature oocytes (Fig. 4C), suggesting that *mos* RNA granules were disassembled during oocyte maturation as in the case of *cyclin B1* RNA granules (Kotani et al., 2013).

The changes in RNA granules were further analyzed by the time course of oocyte maturation. Although the timing of GVBD after induction of maturation varied in oocytes derived from different females (from 90 to 180 min), the *cyclin B1* RNA granules rapidly and simultaneously disassembled in a short period after induction of oocyte maturation (120 min in this batch; Fig. 5A), consistent with the changes reported previously (Kotani et al., 2013; Nukada et al., 2015). In contrast, disassembly of *mos* RNA granules was observed slightly earlier than that of *cyclin B1* RNA granules (90 min in this batch; Fig. 5A and B). In addition to the timing, changes in the number of *mos* RNA granules were different from those of *cyclin B1* RNA granules, i.e., a fraction of *mos* RNA granules firstly disappeared in the early period (90 min) before the onset of GVBD and a large part of them disappeared in a later period (120-150 min) (Fig. 5A-C). These results suggest that the disassembly of *mos* and *cyclin B1* RNA granules is regulated by different mechanisms.

3.5. Temporal control of *mos* mRNA polyadenylation during oocyte maturation

We then examined the changes in poly(A) tail lengths of *mos* and *cyclin B1* mRNAs during zebrafish oocyte maturation by the poly(A) test (PAT) assay. The poly(A) tails of *cyclin B1* mRNA were partially elongated at 90 min and then fully elongated in oocytes 180 min after induction of oocyte maturation (Fig. 6B), consistent with results reported previously (Kotani et al., 2013; Yasuda et al., 2010; Zhang and Sheets, 2009).

The PAT assay of zebrafish *mos* mRNA showed that the poly(A) tails of *mos* mRNA were elongated 60 min after induction of maturation (Fig. 6A), earlier than that of polyadenylation of *cyclin B1* mRNA (90 min) and before the onset of GVBD (Fig. 6A-C). The *mos* mRNA poly(A) tails seemed to be elongated until 150 min and then partially shortened at 180 min after induction of maturation, consistent with observations in *Xenopus* oocytes (Sheets et al., 1994). Taken together, the results suggest that the *mos* mRNA is translationally activated earlier than that of the *cyclin B1* mRNA during zebrafish oocyte maturation.

3.6. Effect of actin filament stabilization on *mos* RNA granules

We finally examined the relationship between the oocyte cytoskeleton and cytoplasmic regulation of *mos* RNA granules. We previously showed that actin filaments that assembled in the oocyte cytoplasm are gradually depolymerized from 20 min after induction of oocyte maturation (Nukada et al., 2015) and that disassembly of *cyclin B1* RNA granules is dependent on depolymerization of actin filaments (Kotani et al., 2013). To stabilize actin filaments, immature oocytes were treated with jasplakinolide, which prevents depolymerization of actin filaments, and stimulated with MIH for 3 h. As reported previously (Kotani et al., 2013), the *cyclin B1* RNA granules were maintained in oocytes treated with jasplakinolide and MIH (Fig. 7C), while *cyclin B1* RNA granules were almost completely dispersed in control oocytes treated with DMSO and MIH (Fig. 7B). Similar to *cyclin B1* RNA granules, some fractions of *mos* RNA granules were maintained in oocytes treated with jasplakinolide and MIH, while certain fractions of them disappeared (Fig. 7C and D). In addition, the PAT assay showed that poly(A) tails of *mos* mRNA were polyadenylated in oocytes treated with jasplakinolide and MIH (Fig. 7E), suggesting translational activation of *mos* mRNA in the oocytes. These results demonstrate that the disassembly of *mos* RNA granules was partially dependent on depolymerization of actin filaments but that certain fractions of them were disassembled independently of actin filaments.

4. Discussion

4.1. Distinct RNA granule formation in vertebrate oocytes

In nematodes, several types of RNA granules have been observed in the cytoplasm of different stages of oocytes. *Caenorhabditis elegans* oocytes form germ granules and processing body (P body)-like granules, which are compositionally different and contain different sets of dormant mRNAs (Boag et al., 2008; Noble et al., 2008; Schisa et al., 2001). In contrast to nematode oocytes, only a few granules containing mRNAs have been observed in vertebrate oocytes. Germinal granules that have assembled in the vegetal polar cytoplasm of the *Xenopus* oocyte contain dormant mRNAs such as Xcat2, Xpat and DEADSouth, which are thought to be translated during development and play important roles in germ cell development (Kloc et al., 2002). We previously demonstrated that dormant *cyclin B1* mRNA form RNA granules in the animal polar cytoplasm of the zebrafish oocyte (Kotani et al., 2013). Translational control of this mRNA is important for progression of oocyte maturation. In this study, we found that dormant *mos* mRNA also forms RNA granules in the animal polar cytoplasm of zebrafish oocytes (Fig. 1). This mRNA is translationally activated at a timing different from that of *cyclin B1* in fish and frog (Kajiura-Kobayashi et al., 2000; Kobayashi et al., 1991; Kondo et al., 2001; Sagata et al., 1989). An intriguing finding in the present study was that *mos* RNA granules were different from those of *cyclin B1* despite the fact that both types of granules were localized in similar regions of the oocyte cytoplasm beneath the micropyle (Fig. 2). Our results show for the first time that vertebrate oocytes deposit dormant mRNAs by assembling distinct types of RNA granules in a restricted region of the cytoplasm.

The mechanism of the formation of *mos* RNA granules remains unknown. One of the known elements involved in RNA granule formation is Pumilio-binding element (PBE) in the 3'UTR of *cyclin B1* mRNA (Kotani et al., 2013). A reporter mRNA containing full-length *cyclin B1* formed granules in the oocyte cytoplasm, while that carrying mutations on PBE did not. Binding of Pumilio1 to the reporter mRNA was abolished by the mutations on PBE, suggesting that Pumilio1 promotes the formation of *cyclin B1* RNA granules (Kotani et al., 2013). Indeed, *Drosophila* Pumilio has the ability to form ordered aggregations of the proteins (Salazar et al., 2010). Although zebrafish *mos* mRNA contains a putative PBE in its 3'UTR, no binding between *mos* mRNA and Pumilio1 *in vivo* was shown in our previous study (Kotani et al., 2013). Therefore, Pumilio1 would not be involved in the formation of *mos* RNA granules. In terms of *trans*-acting factors, cytoplasmic polyadenylation element-binding protein (CPEB) is

one of the candidates for promoting the formation of *mos* RNA granules, because *Aplysia* and *Drosophila* CPEBs form ordered aggregations (Majumdar et al., 2012; Si et al., 2010) and zebrafish *mos* mRNA contains CPEs in its 3'UTR and binds to CPEB (Suzuki et al., 2009). However, given that CPEB was involved in the granule formation, distinct RNA granules would be assembled by additional factors, because both *cyclin B1* and *mos* mRNAs contain CPEs in their 3'UTR.

In neuronal cells, several types of RNA granules have been identified. Many mRNAs transcribed in these cells are assembled into distinct granules and localized in dendrites (Baez et al., 2011; Mikl et al., 2011). Large-scale analysis of proteins interacting with Barentsz and Staufen2, components of neuronal RNA granules, showed that each protein forms large complexes with a partially similar set of, but largely different sets of, proteins with distinct target mRNAs (Fritzsche et al., 2013). In this study, we demonstrated that *in vitro* synthesized *mos* and *cyclin B1* RNAs exhibit low densities, while *mos* and *cyclin B1* RNA granules in oocytes exhibit different and high densities in sucrose density ultracentrifugation analysis (Fig. 3). These results suggest that *mos* and *cyclin B1* RNA granules form large complexes consisting of different components as in the case of neuronal RNA granules. Some of the known components such as Pumilio1 and insulin-like growth factor 2 mRNA-binding protein 3 (IMP3) for *cyclin B1* granules and CPEB for both types of granules were distributed in heavy fractions similar to *mos* and *cyclin B1* mRNAs (Takahashi et al., 2014). To understand the mechanisms of distinct RNA granule formation, components consisting of distinct RNA granules need to be identified in future studies.

4.2. Cytoplasmic polyadenylation of *mos* mRNA during zebrafish oocyte maturation

Cytoplasmic polyadenylation of *mos* mRNA has been shown to direct translational activation of this mRNA in frog and mouse (Charlesworth et al., 2002; Gebauer et al., 1994; Sheets et al., 1994). In this study, we demonstrated cytoplasmic polyadenylation of *mos* mRNA in an early period after induction of oocyte maturation in zebrafish (Fig. 6). Although we could not detect Mos protein in zebrafish, the timing of Mos synthesis during oocyte maturation was demonstrated in goldfish and is almost the same as the timing of cytoplasmic poyadenylation of *mos* mRNA in zebrafish oocyte maturation, i.e., Mos synthesis begins in an early period before MPF activation and GVBD

(Kajiura-Kobayashi et al., 2000). Therefore, cytoplasmic polyadenylation of *mos* mRNA would be closely related to translational activation of the mRNA in zebrafish.

The *cis*-acting element CPE and its binding protein CPEB direct translational repression and activation of *mos* mRNA in *Xenopus* and mouse oocytes (Gebauer et al., 1994; Mendez and Richter, 2001; Sheets et al., 1994). In addition to CPE, *Xenopus mos* mRNA contains MBE in the 3'UTR. Musashi binds to the MBE and directs translational activation of *mos* mRNA in an early period of *Xenopus* oocyte maturation (Charlesworth et al., 2002; Charlesworth et al., 2006). Cytoplasmic polyadenylation of *mos* mRNA was also demonstrated in human oocytes. Interestingly, human *mos* mRNA contains CPE but not MBE, and a reporter mRNA of human *mos* is translated in a late period during oocyte maturation in *Xenopus* oocytes, showing species-specific differences that would be dependent on *cis*-acting elements and suggesting the importance of MBE for translational activation of the mRNA in an early period (Prasad et al., 2008). Since zebrafish *mos* mRNA has a putative MBE in its 3'UTR, it is possible that cytoplasmic polyadenylation of *mos* mRNA is directed by MBE in the early period of zebrafish oocyte maturation. Involvement of MBE and Musashi in translational control of zebrafish *mos* mRNA is an interesting issue and remains to be investigated.

4.3. Temporal control of mRNA translation by formation and disassembly of RNA granules

FISH analysis of oocytes after induction of oocyte maturation showed that *mos* RNA granules began to disassemble at the timing that coincided with the cytoplasmic polyadenylation of mRNA (Figs. 4, 5 and 6), as in the case of *cyclin B1* RNA granules (Kotani et al., 2013). These results suggest that disassembly of RNA granules resulted in translational activation of the mRNA. In support of this notion, recent studies have demonstrated that RNA granules are selectively disassembled in response to specific signals and that this change is related to subsequent translational activation of the assembled mRNAs. In *Drosohila* oocytes, processing body-like granules are assembled in the anterior region of oocytes with *bicoid* mRNA, which encodes a protein required for embryonic axis formation (Weil et al., 2012). These granules are dispersed after fertilization, resulting in translational activation of *bicoid* mRNA and embryonic axis formation. Neuronal RNA granules containing the translational repressor Smaug1 are localized at synapses and are disassembled by stimulation of the N-methyl-D-aspartic

acid (NMDA) receptor (Baez et al., 2011). The Smaug1 target mRNAs are dissociated and subsequently translated in the synapses, leading to synaptic plasticity. Importantly, distinct neuronal RNA granules are independently disassembled by different neuronal stimuli, suggesting that translational activation of a subset of mRNAs is regulated by the formation and disassembly of distinct granules (Baez et al., 2011; Luchelli et al., 2015; Mikl et al., 2011). The *mos* and *cyclin B1* RNA granules that assembled in the animal polar cytoplasm of zebrafish oocytes were disassembled after induction of oocyte maturation by stimulation with MIH at slightly different timings, which coincided with the cytoplasmic polyadenylation of distinct mRNAs (Figs. 5 and 6) (Kotani et al., 2013). In addition, *mos* RNA granules were disassembled in a manner distinguishable from that of *cyclin B1* RNA granules (Fig. 5). Our results suggest that distinct RNA granules could be independently regulated for achieving translational control of distinct mRNAs in temporal order that is important for progression of oocyte maturation.

We previously showed that assembly and disassembly of *cyclin B1* RNA granules are dependent on polymerization and depolymerization of actin filaments (Kotani et al., 2013; Nukada et al., 2015). Disassembly of some, but not all, of the fractions of *mos* RNA granules was also dependent on actin filaments (Fig. 7). However, disassembly of certain fractions of *mos* RNA granules was independent of actin filaments (Fig. 7). This actin filament-independent disassembly may promote translational activation of *mos* mRNA in the early period during oocyte maturation, because a reporter mRNA of *cyclin B1* localized in the animal polar cytoplasm and anchored there via actin filaments is translated at a timing similar to that of endogenous *cyclin B1* mRNA, while mutant reporter mRNA distributed in the cytoplasm in a manner independent of actin filaments is translated in an early period after induction of oocyte maturation (Yasuda et al., 2010; Yasuda et al., 2013). Another explanation is that the *mos* RNA granules for which disassembly is independent of actin filaments are fluid and sensitive to signaling downstream of the MIH receptor, while some fractions of the granules are stably anchored to actin filaments and require depolymerization of the filaments to disassemble. Nevertheless, our results show the existence of heterogeneity in *mos* RNA granules, which would exert the gradual synthesis of Mos protein observed in goldfish oocyte maturation (Kajiura-Kobayashi et al., 2000).

5. Conclusion

We demonstrated for the first time that dormant mRNAs encoding proteins promoting the meiotic cell cycle form distinct RNA granules in the cytoplasm of oocytes. Our results provide a novel insight into mRNA regulation at the subcellular level and suggest that the formation and disassembly of distinct RNA granules contributes to the temporal control of translational activation of distinct mRNAs. Future studies including analyses of cytoplasmic regulation of other mRNAs that play important roles in the meiotic cell cycle and embryonic development will contribute to an understanding of the mechanisms by which oocytes promote reproductive and developmental processes during oogenesis and early development.

Acknowledgements

This work was supported by Grant-in-Aid for Scientific Research (25440001 and 16K07242 to T.K.) from the Ministry of Education, Culture, Sports, Science and Technology, Japan.

References

Araki, K., Naito, K., Haraguchi, S., Suzuki, R., Yokoyama, M., Inoue, M., Aizawa, S., Toyoda, Y., Sato, E., 1996. Meiotic abnormalities of c-mos knockout mouse oocytes: activation after first meiosis or entrance into third meiotic metaphase. Biol. Reprod. 55, 1315-1324.

Baez, M.V., Luchelli, L., Maschi, D., Habif, M., Pascual, M., Thomas, M.G., Boccaccio, G.L., 2011. Smaug1 mRNA-silencing foci respond to NMDA and modulate synapse formation. J. Cell Biol. 195, 1141-1157.

Barkoff, A.F., Dickson, K.S., Gray, N.K., Wickens, M., 2000. Translational control of cyclin B1 mRNA during meiotic maturation: coordinated repression and cytoplasmic polyadenylation. Dev. Biol. 220, 97-109.

Boag, P.R., Atalay, A., Robida, S., Reinke, V., Blackwell, T.K., 2008. Protection of specific maternal messenger RNAs by the P body protein CGH-1 (Dhh1/RCK)

during Caenorhabditis elegans oogenesis. J. Cell Biol. 182, 543-557.

Charlesworth, A., Cox, L.L., MacNicol, A.M., 2004. Cytoplasmic polyadenylation element (CPE)- and CPE-binding protein (CPEB)-independent mechanisms regulate early class maternal mRNA translational activation in Xenopus oocytes. J. Biol. Chem. 279, 17650-17659.

Charlesworth, A., Ridge, J.A., King, L.A., MacNicol, M.C., MacNicol, A.M., 2002. A novel regulatory element determines the timing of Mos mRNA translation during Xenopus oocyte maturation. EMBO J. 21, 2798-2806.

Charlesworth, A., Wilczynska, A., Thampi, P., Cox, L.L., MacNicol, A.M., 2006. Musashi regulates the temporal order of mRNA translation during Xenopus oocyte maturation. EMBO J. 25, 2792-2801.

Choi, T., Fukasawa, K., Zhou, R., Tessarollo, L., Borror, K., Resau, J., Vande Woude, G.F., 1996. The Mos/mitogen-activated protein kinase (MAPK) pathway regulates the size and degradation of the first polar body in maturing mouse oocytes. Proc. Natl. Acad. Sci. USA 93, 7032-7035.

Davydenko, O., Schultz, R.M., Lampson, M.A., 2013. Increased CDK1 activity determines the timing of kinetochore-microtubule attachments in meiosis I. J. Cell Biol. 202, 221-229.

de Moor, C.H., Meijer, H., Lissenden, S., 2005. Mechanisms of translational control by the 3' UTR in development and differentiation. Semin. Cell Dev. Biol. 16, 49-58.

de Moor, C.H., Richter, J.D., 1999. Cytoplasmic polyadenylation elements mediate masking and unmasking of cyclin B1 mRNA. EMBO J. 18, 2294-2303.

Dupre, A., Jessus, C., Ozon, R., Haccard, O., 2002. Mos is not required for the initiation of meiotic maturation in Xenopus oocytes. EMBO J. 21, 4026-4036.

Fisher, D.L., Brassac, T., Galas, S., Doree, M., 1999. Dissociation of MAP kinase activation and MPF activation in hormone-stimulated maturation of Xenopus oocytes. Development 126, 4537-4546.

Fritzsche, R., Karra, D., Bennett, K.L., Ang, F.Y., Heraud-Farlow, J.E., Tolino, M., Doyle, M., Bauer, K.E., Thomas, S., Planyavsky, M., Arn, E., Bakosova, A., Jungwirth, K., Hormann, A., Palfi, Z., Sandholzer, J., Schwarz, M., Macchi, P., Colinge, J., Superti-Furga, G., Kiebler, M.A., 2013. Interactome of two diverse RNA granules links mRNA localization to translational repression in neurons. Cell Rep. 5, 1749-1762.

Gebauer, F., Xu, W., Cooper, G.M., Richter, J.D., 1994. Translational control by cytoplasmic polyadenylation of c-mos mRNA is necessary for oocyte maturation in the mouse. EMBO J. 13, 5712-5720.

Gross, S.D., Schwab, M.S., Taieb, F.E., Lewellyn, A.L., Qian, Y.W., Maller, J.L., 2000. The critical role of the MAP kinase pathway in meiosis II in Xenopus oocytes is mediated by p90(Rsk). Curr. Biol. : CB 10, 430-438.

Hochegger, H., Klotzbucher, A., Kirk, J., Howell, M., le Guellec, K., Fletcher, K., Duncan, T., Sohail, M., Hunt, T., 2001. New B-type cyclin synthesis is required between meiosis I and II during Xenopus oocyte maturation. Development 128, 3795-3807.

Ihara, J., Yoshida, N., Tanaka, T., Mita, K., Yamashita, M., 1998. Either cyclin B1 or B2 is necessary and sufficient for inducing germinal vesicle breakdown during frog (Rana japonica) oocyte maturation. Mol. Reprod. Dev. 50, 499-509.

Kajiura-Kobayashi, H., Yoshida, N., Sagata, N., Yamashita, M., Nagahama, Y., 2000. The Mos/MAPK pathway is involved in metaphase II arrest as a cytostatic factor but is neither necessary nor sufficient for initiating oocyte maturation in goldfish. Dev. Genes Evol. 210, 416-425.

Kloc, M., Dougherty, M.T., Bilinski, S., Chan, A.P., Brey, E., King, M.L., Patrick, C.W., Jr., Etkin, L.D., 2002. Three-dimensional ultrastructural analysis of RNA distribution within germinal granules of Xenopus. Dev. Biol. 241, 79-93.

Kobayashi, H., Minshull, J., Ford, C., Golsteyn, R., Poon, R., Hunt, T., 1991. On the synthesis and destruction of A- and B-type cyclins during oogenesis and meiotic maturation in Xenopus laevis. J. Cell Biol. 114, 755-765.

Kondo, T., Kotani, T., Yamashita, M., 2001. Dispersion of cyclin B mRNA aggregation is coupled with translational activation of the mRNA during zebrafish oocyte maturation. Dev. Biol. 229, 421-431.

Kondo, T., Yanagawa, T., Yoshida, N., Yamashita, M., 1997. Introduction of cyclin B induces activation of the maturation-promoting factor and breakdown of germinal vesicle in growing zebrafish oocytes unresponsive to the maturation-inducing hormone. Dev. Biol. 190, 142-152.

Kotani, T., Yamashita, M., 2002. Discrimination of the roles of MPF and MAP kinase in morphological changes that occur during oocyte maturation. Dev. Biol. 252, 271-286.

Kotani, T., Yasuda, K., Ota, R., Yamashita, M., 2013. Cyclin B1 mRNA translation is temporally controlled through formation and disassembly of RNA granules. J. Cell Biol. 202, 1041-1055.

Ledan, E., Polanski, Z., Terret, M.E., Maro, B., 2001. Meiotic maturation of the mouse oocyte requires an equilibrium between cyclin B synthesis and degradation. Dev. Biol. 232, 400-413.

Luchelli, L., Thomas, M.G., Boccaccio, G.L., 2015. Synaptic control of mRNA translation by reversible assembly of XRN1 bodies. J. Cell Sci. 128, 1542-1554.

Majumdar, A., Cesario, W.C., White-Grindley, E., Jiang, H., Ren, F., Khan, M.R., Li, L., Choi, E.M., Kannan, K., Guo, F., Unruh, J., Slaughter, B., Si, K., 2012. Critical role of amyloid-like oligomers of Drosophila Orb2 in the persistence of memory. Cell 148, 515-529.

Masui, Y., Clarke, H.J., 1979. Oocyte maturation. Int. Rev. Cytol. 57, 185-282.

McGrew, L.L., Dworkin-Rastl, E., Dworkin, M.B., Richter, J.D., 1989. Poly(A) elongation during Xenopus oocyte maturation is required for translational recruitment and is mediated by a short sequence element. Genes Dev. 3, 803-815.

Mendez, R., Richter, J.D., 2001. Translational control by CPEB: a means to the end. Nature reviews. Mol. Cell Biol. 2, 521-529.

Mikl, M., Vendra, G., Kiebler, M.A., 2011. Independent localization of MAP2, CaMKIIalpha and beta-actin RNAs in low copy numbers. EMBO Rep. 12, 1077-1084.

Nakahata, S., Katsu, Y., Mita, K., Inoue, K., Nagahama, Y., Yamashita, M., 2001. Biochemical identification of Xenopus Pumilio as a sequence-specific cyclin B1 mRNA-binding protein that physically interacts with a Nanos homolog, Xcat-2, and a cytoplasmic polyadenylation element-binding protein. J. Biol. Chem. 276, 20945-20953.

Nakahata, S., Kotani, T., Mita, K., Kawasaki, T., Katsu, Y., Nagahama, Y., Yamashita, M., 2003. Involvement of Xenopus Pumilio in the translational regulation that is specific to cyclin B1 mRNA during oocyte maturation. Mech. Dev. 120, 865-880.

Noble, S.L., Allen, B.L., Goh, L.K., Nordick, K., Evans, T.C., 2008. Maternal mRNAs are regulated by diverse P body-related mRNP granules during early Caenorhabditis elegans development. J. Cell Biol. 182, 559-572.

Nukada, Y., Horie, M., Fukui, A., Kotani, T., Yamashita, M., 2015. Real-time imaging of actin filaments in the zebrafish oocyte and embryo. Cytoskeleton (Hoboken) 72, 491-501.

Nurse, P., 1990. Universal control mechanism regulating onset of M-phase. Nature 344, 503-508.

Ota, R., Kotani, T., Yamashita, M., 2011. Biochemical characterization of Pumilio1 and Pumilio2 in Xenopus oocytes. J. Biol. Chem. 286, 2853-2863.

Pique, M., Lopez, J.M., Foissac, S., Guigo, R., Mendez, R., 2008. A combinatorial code for CPE-mediated translational control. Cell 132, 434-448.

Prasad, C.K., Mahadevan, M., MacNicol, M.C., MacNicol, A.M., 2008. Mos 3' UTR regulatory differences underlie species-specific temporal patterns of Mos mRNA cytoplasmic polyadenylation and translational recruitment during oocyte maturation. Mol. Reprod. Dev. 75, 1258-1268.

Sagata, N., Daar, I., Oskarsson, M., Showalter, S.D., Vande Woude, G.F., 1989. The product of the mos proto-oncogene as a candidate "initiator" for oocyte maturation. Science 245, 643-646.

Salazar, A.M., Silverman, E.J., Menon, K.P., Zinn, K., 2010. Regulation of synaptic Pumilio function by an aggregation-prone domain. J. Neurosci. 30, 515-522.

Schisa, J.A., Pitt, J.N., Priess, J.R., 2001. Analysis of RNA associated with P granules in germ cells of C. elegans adults. Development 128, 1287-1298.

Sheets, M.D., Fox, C.A., Hunt, T., Vande Woude, G., Wickens, M., 1994. The 3'-untranslated regions of c-mos and cyclin mRNAs stimulate translation by regulating cytoplasmic polyadenylation. Genes Dev. 8, 926-938.

Si, K., Choi, Y.B., White-Grindley, E., Majumdar, A., Kandel, E.R., 2010. Aplysia CPEB can form prion-like multimers in sensory neurons that contribute to long-term facilitation. Cell 140, 421-435.

Suzuki, H., Tsukahara, T., Inoue, K., 2009. Localization of c-mos mRNA around the animal pole in the zebrafish oocyte with Zor-1/Zorba. Biosci. Trends 3, 96-104.

Takahashi, K., Kotani, T., Katsu, Y., Yamashita, M., 2014. Possible involvement of insulin-like growth factor 2 mRNA-binding protein 3 in zebrafish oocyte maturation as a novel cyclin B1 mRNA-binding protein that represses the translation in immature oocytes. Biochem. Biophy. Res. Commun. 448, 22-27.

Tanaka, T., Yamashita, M., 1995. Pre-MPF is absent in immature oocytes of fishes and

amphibians except Xenopus. Dev. Growth Differ. 37, 387-393.

Tay, J., Hodgman, R., Richter, J.D., 2000. The control of cyclin B1 mRNA translation during mouse oocyte maturation. Dev. Biol. 221, 1-9.

Vassalli, J.D., Huarte, J., Belin, D., Gubler, P., Vassalli, A., O'Connell, M.L., Parton, L.A., Rickles, R.J., Strickland, S., 1989. Regulated polyadenylation controls mRNA translation during meiotic maturation of mouse oocytes. Genes Dev. 3, 2163-2171.

Verlhac, M.H., Kubiak, J.Z., Weber, M., Geraud, G., Colledge, W.H., Evans, M.J., Maro, B., 1996. Mos is required for MAP kinase activation and is involved in microtubule organization during meiotic maturation in the mouse. Development 122, 815-822.

Weil, T.T., Parton, R.M., Herpers, B., Soetaert, J., Veenendaal, T., Xanthakis, D., Dobbie, I.M., Halstead, J.M., Hayashi, R., Rabouille, C., Davis, I., 2012. Drosophila patterning is established by differential association of mRNAs with P bodies. Nature Cell Biol. 14, 1305-1313.

Yasuda, K., Kotani, T., Ota, R., Yamashita, M., 2010. Transgenic zebrafish reveals novel mechanisms of translational control of cyclin B1 mRNA in oocytes. Dev. Biol. 348, 76-86.

Yasuda, K., Kotani, T., Yamashita, M., 2013. A cis-acting element in the coding region of cyclin B1 mRNA couples subcellular localization to translational timing. Dev. Biol. 382, 517-529.

Zhang, Y., Sheets, M.D., 2009. Analyses of zebrafish and Xenopus oocyte maturation reveal conserved and diverged features of translational regulation of maternal cyclin B1 mRNA. BMC Dev. Biol. 9, 7.

Figure legends

Fig. 1. Dormant *mos* mRNA is stored as RNA granules localized in the animal polar cytoplasm of zebrafish oocytes. (A) Distribution of *mos* mRNA in the zebrafish oocyte. GV, germinal vesicle; m, micropyle; f, follicle cells; c, chorion. (B and C) FISH analysis of *mos* mRNA (green) in the zebrafish oocyte using the full length of the antisense *mos* RNA probe. DNA is shown in blue. C is an enlarged view of the boxed region in B. (D) Schematic views for *mos* mRNA (*mos*) and antisense *mos* RNA probes consisting of full-length (Full), 5' half (5') and 3'half (3') of *mos* sequences. (E and F) FISH analysis of *mos* mRNA (green) in the zebrafish oocyte using the (E) 5' half or (F) 3' half of the antisense *mos* RNA probe. Bars: 50 μm in A, 10 μm in B, C, E and F.

Fig. 2. Dormant *mos* and *cyclin B1* mRNAs are stored as distinct RNA granules localized in similar regions of the animal polar cytoplasm of zebrafish oocytes. (A, B and C) FISH analysis of (A) *mos* (green) and (B) *cyclin B1* (red) mRNAs in the zebrafish oocyte using DIG-labeled antisense *mos* and fluorescein-labeled antisense *cyclin B1* RNA probes. A merged image is shown in C. DNA is shown in blue. The *mos* and *cyclin B1* RNA granules were distributed in similar regions of the animal polar cytoplasm. m, micropyle; f, follicle cells; c, chorion. (D, E and F) Enlarged views of the boxed regions in A, B and C. The *mos* and *cyclin B1* RNA granules were distributed in the oocyte cytoplasm as different granules. (G, H and I) FISH analysis of (G) *mos* (red) and (H) *cyclin B1* (green) mRNAs in the oocyte using fluorescein-labeled antisense *mos* and DIG-labeled antisense *cyclin B1* RNA probes. A merged image is shown in I. DNA is shown in blue. Bars: 10 μm.

Fig. 3. Density of *mos* RNA granules is partly lower than that of *cyclin B1* RNA granules. (A) Sucrose density ultracentrifugation analysis of zebrafish ovary extracts. The extracts were dissected into 10 fractions from top (left, 5%) to bottom (right, 65%) after centrifugation. The distribution of proteins was analyzed by CBB staining (top). The distribution of Rpl11 was analyzed by immunoblotting (bottom). (B) Sucrose density ultracentrifugation analysis of fluorescein dextran of 500,000 molecular weight. (C) Sucrose density ultracentrifugation analysis of ovary extracts. The amounts of *mos* (circles) and *cyclin B1* (squares) mRNAs in distinct fractions were analyzed by quantitative RT-PCR (means ± standard deviations; n = 3). The results obtained in three

independent experiments are summarized. Student's *t*-test of the percentages of *mos* and *cyclin B1* mRNAs: **P* < 0.05. (D) Sucrose density ultracentrifugation analysis of *in vitro* synthesized *mos* and *cyclin B1* RNAs. The amounts of *mos* (circles) and *cyclin B1* (squares) RNAs in distinct fractions were analyzed by quantitative RT-PCR. Similar results were obtained from two independent experiments. (E and F) Sucrose density ultracentrifugation analysis of oocytes treated with puromycin. (E) The distribution of Rpl11 and (F) the amounts of *mos* (circles) and *cyclin B1* (squares) mRNAs. Similar results were obtained from two independent experiments.

Fig. 4. *mos* RNA granules are disassembled during oocyte maturation. (A and B) FISH analysis of *mos* mRNA in (A) immature and (B) mature oocytes. m, micropyle; f, follicle cells; c, chorion. The *mos* RNA granules almost completely disappeared during oocyte maturation. Similar results were obtained from three independent experiments. Bars: 10 μm. (C) *mos* mRNA from equal numbers of immature (Im) and mature (M) oocytes were assayed by quantitative RT-PCR (means ± standard deviations; n = 3).

Fig. 5. *mos* RNA granules are gradually disassembled during oocyte maturation. (A) FISH analysis of *mos* (green, top) and *cyclin B1* (red, middle) mRNAs in oocytes 30, 60, 90, 120 and 150 min after induction of oocyte maturation. Merged images are shown at the bottom (Merge). DNA is shown in blue. The *mos* RNA granules gradually disappeared from 90 min after induction of oocyte maturation, while the *cyclin B1* RNA granules rapidly disappeared at 120 min. f, follicle cells; c, chorion. Bars: 10 μm. (B) The number of *mos* RNA granules in 100 μm^2 of cytoplasm was counted (means ± standard deviations; n = 6). Student's *t*-test relative to the point at 0 min: **P* < 0.05, ***P* < 0.01. (C) Time course of GVBD after MIH stimulation. Similar results were obtained from two independent experiments.

Fig. 6. Poly(A) tails of *mos* mRNA are elongated in an early period during oocyte maturation. (A and B) Time courses of polyadenylation of (A) *mos* and (B) *cyclin B1* mRNAs. Dotted lines indicate the basal size of poly(A) tails. Bars indicate elongated poly(A) tails. The intensities of signals larger than the basal size (dotted lines) are shown at the bottom (relative to the intensity at 0 min). The poly(A) tails of *mos* and *cyclin B1* mRNAs remain short in oocytes 0 min after MIH treatment. Polyadenylation

of *mos* mRNA was initiated at 60 min and that of *cyclin B1* was initiated at 90 min after MIH treatment. (C) Time course of GVBD after MIH stimulation. Similar results were obtained from two independent experiments.

Fig. 7. Disassembly of some, but not all, of the *mos* RNA granules is dependent on actin filament depolymerization. (A, B and C) FISH analysis of *mos* (green, upper) and *cyclin B1* (red, middle) mRNAs in oocytes treated with (A and B) DMSO or (C) jasplakinolide (Jasp) and simultaneously with MIH (B and C). Merged images are shown at the bottom (Merge). DNA is shown in blue. The *mos* and *cyclin B1* RNA granules almost completely disappeared in oocytes treated with DMSO and MIH, while some *mos* RNA granules and large amounts of *cyclin B1* RNA granules were maintained in oocytes treated with jasplakinolide and MIH. f, follicle cells; c, chorion. Bars: 10 μm. (D) The number of *mos* RNA granules in 100 μm^2 of cytoplasm was counted (means ± standard deviations; n = 9) in oocytes treated with (+) or without (-) jasplakinolide (Jasp) and MIH. Student's *t*-test: $^{**}P < 0.01$. (E) PAT assay of *mos* mRNA in oocytes treated with (+) or without (-) jasplakinolide (Jasp) and MIH. Dotted lines indicate the basal size of poly(A) tails. Bars indicate elongated poly(A) tails. Similar results were obtained from two independent experiments.

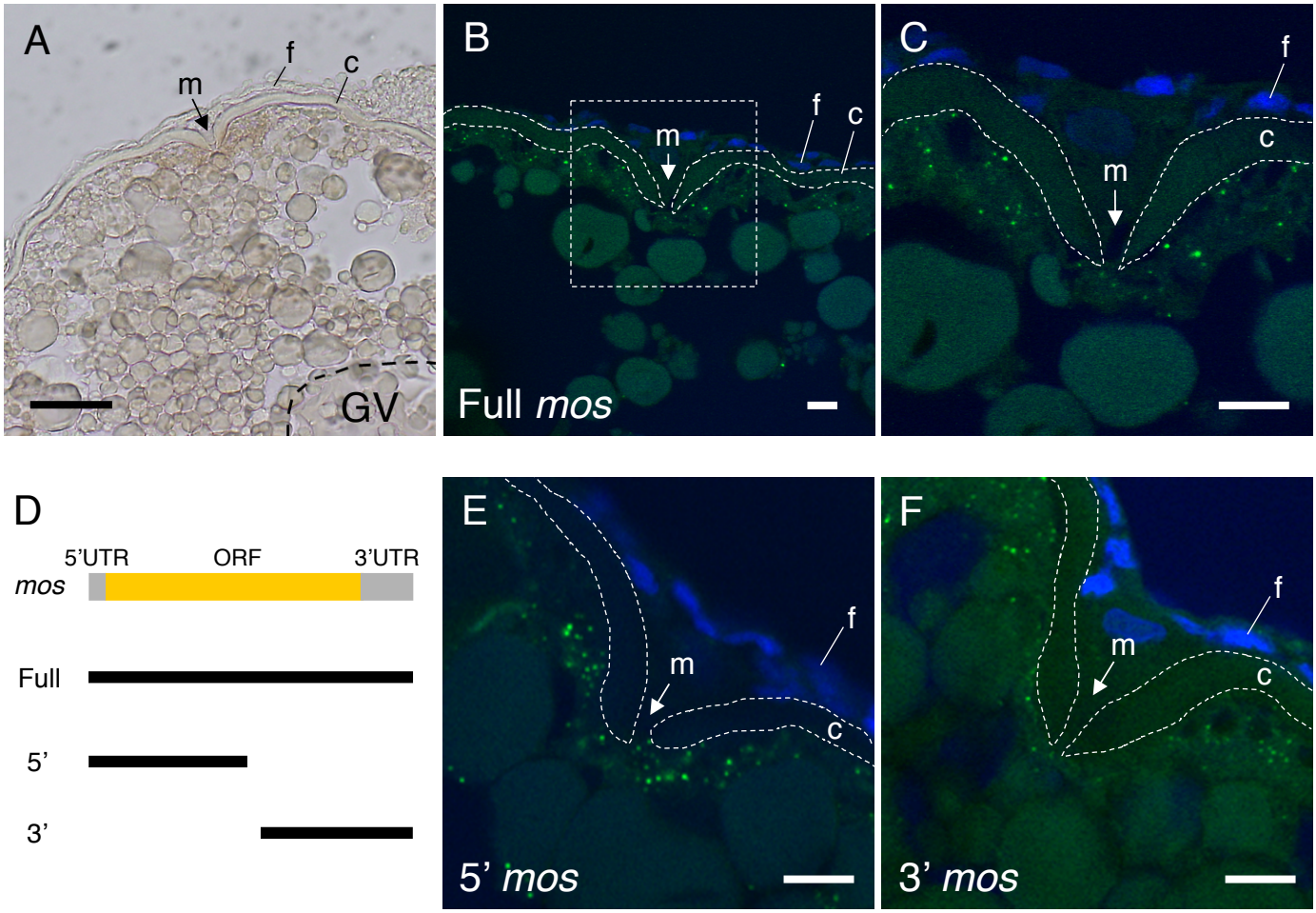
A
m
f
c
GV
B
m
f
c
Full *mos*
C
f
c
m
D
5'UTR
ORF
3'UTR
mos
Full
5'
3'
E
f
m
c
5' *mos*
F
f
m
c
3' *mos*

Fig. 1

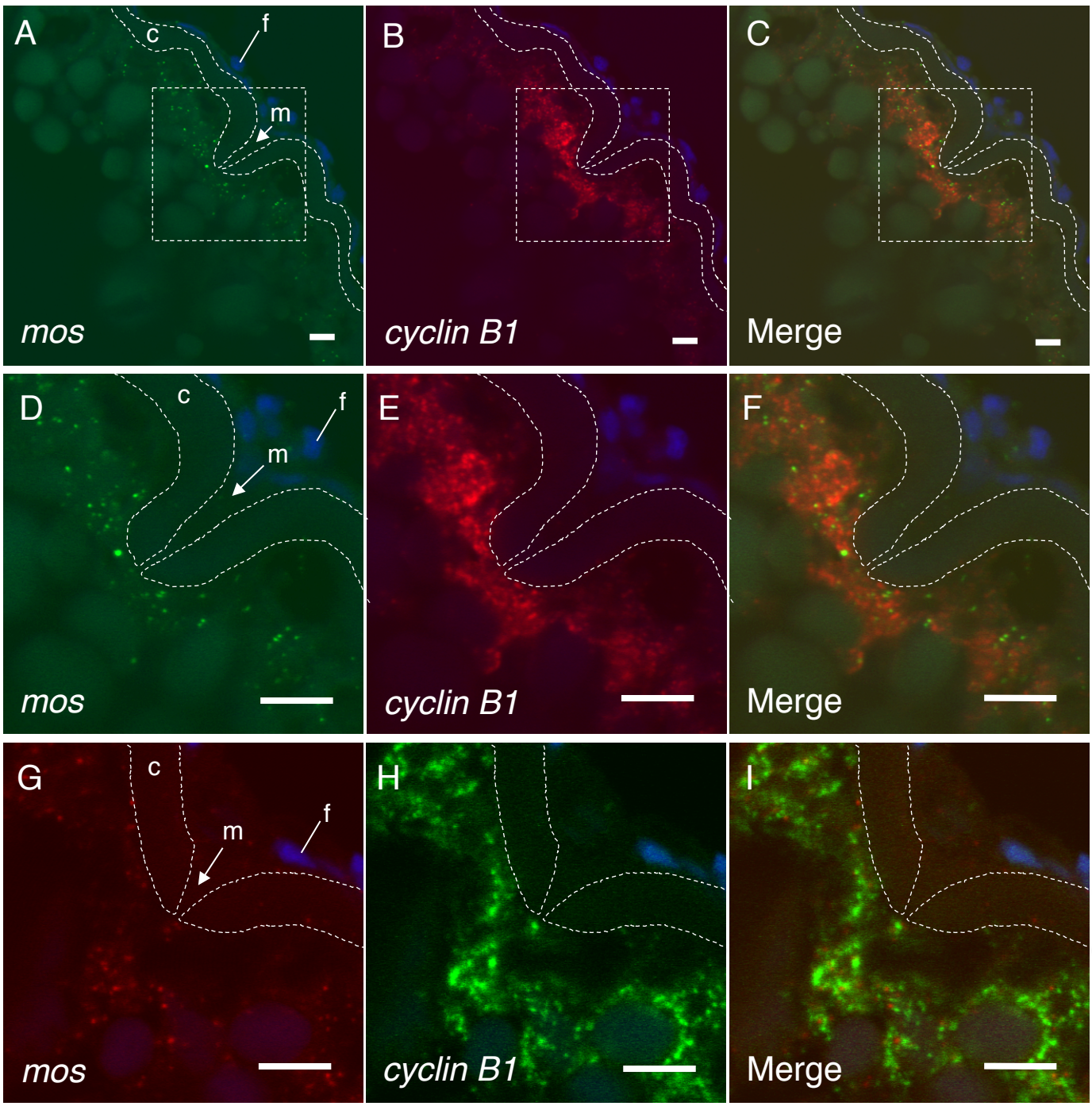
A
c
f
m
mos
B
cyclin B1
C
Merge
D
c
f
m
mos
E
cyclin B1
F
Merge
G
c
m
f
mos
H
cyclin B1
I
Merge

Fig. 2

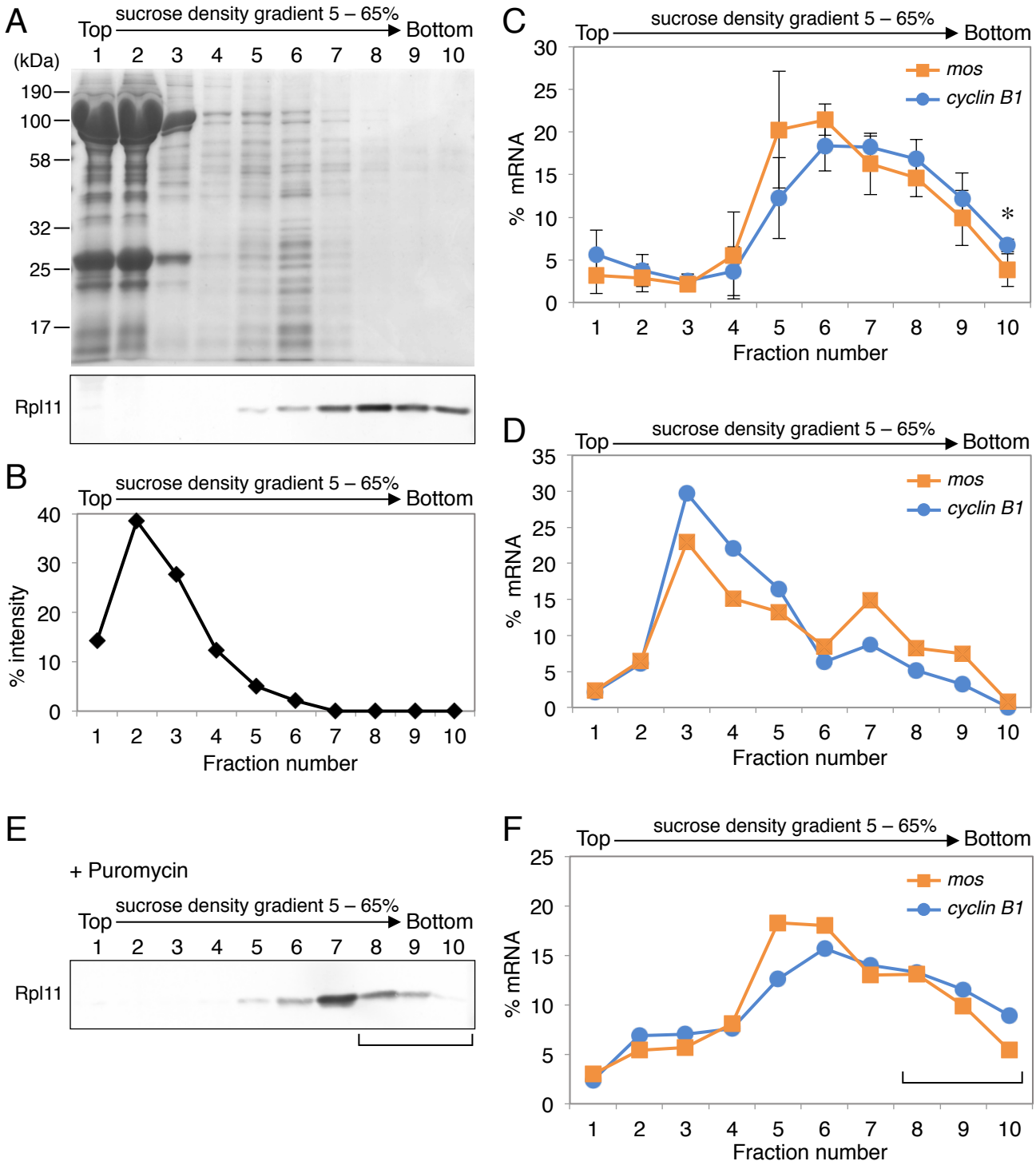
A
sucrose density gradient 5 – 65%
Top
Bottom
(kDa)
1 2 3 4 5 6 7 8 9 10
190
100
58
32
25
17
Rpl11
B
sucrose density gradient 5 – 65%
Top
Bottom
% intensity
Fraction number
C
sucrose density gradient 5 – 65%
Top
Bottom
mos
cyclin B1
% mRNA
Fraction number
*
D
sucrose density gradient 5 – 65%
Top
Bottom
mos
cyclin B1
% mRNA
Fraction number
E
+ Puromycin
sucrose density gradient 5 – 65%
Top
Bottom
Rpl11
F
sucrose density gradient 5 – 65%
Top
Bottom
mos
cyclin B1
% mRNA
Fraction number

Fig. 3

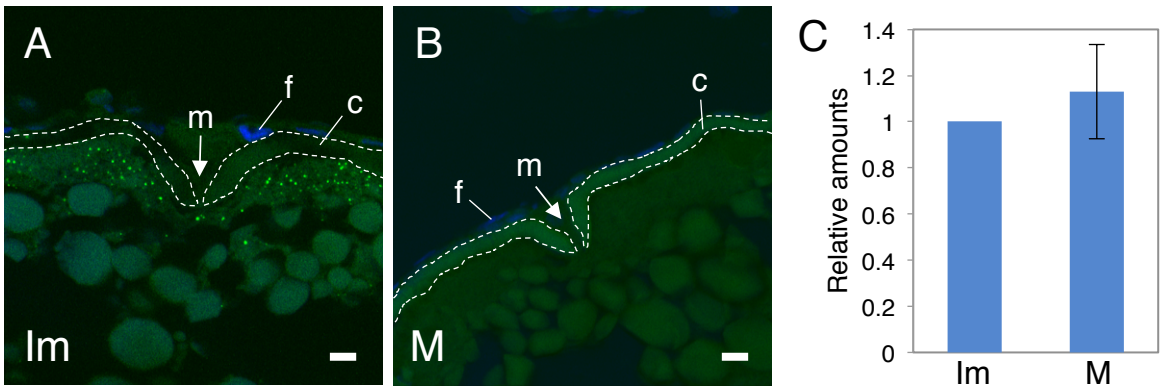

Fig. 4

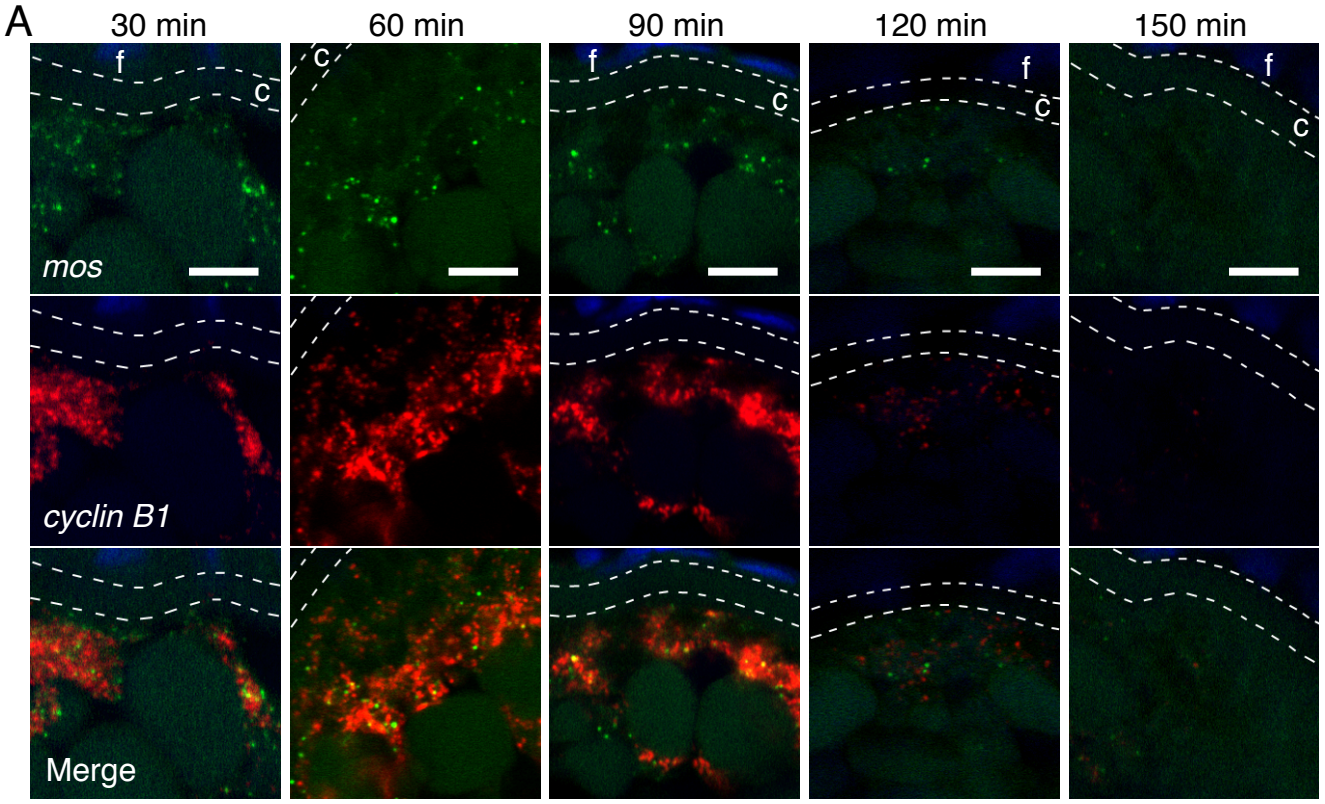
A
30 min
60 min
90 min
120 min
150 min
f
c
mos
cyclin B1
Merge

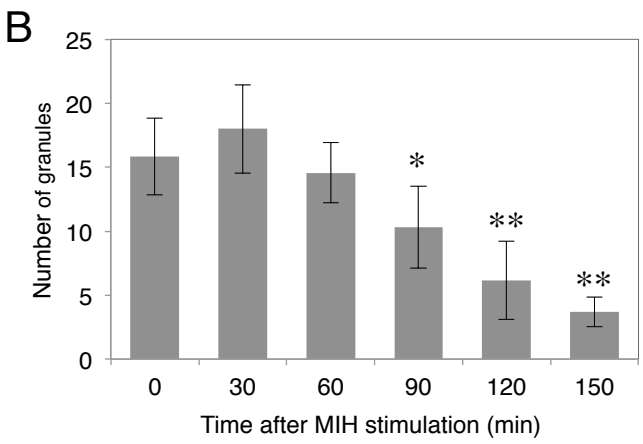
B
Number of granules
25
20
15
10
5
0
*
**
**
0
30
60
90
120
150
Time after MIH stimulation (min)

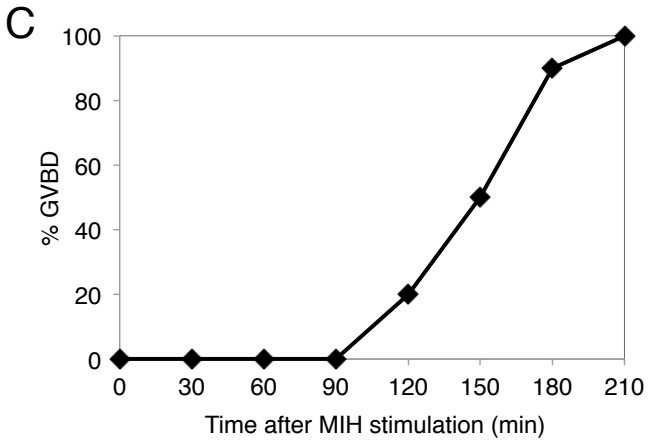
C
% GVBD
100
80
60
40
20
0
0
30
60
90
120
150
180
210
Time after MIH stimulation (min)

Fig. 5

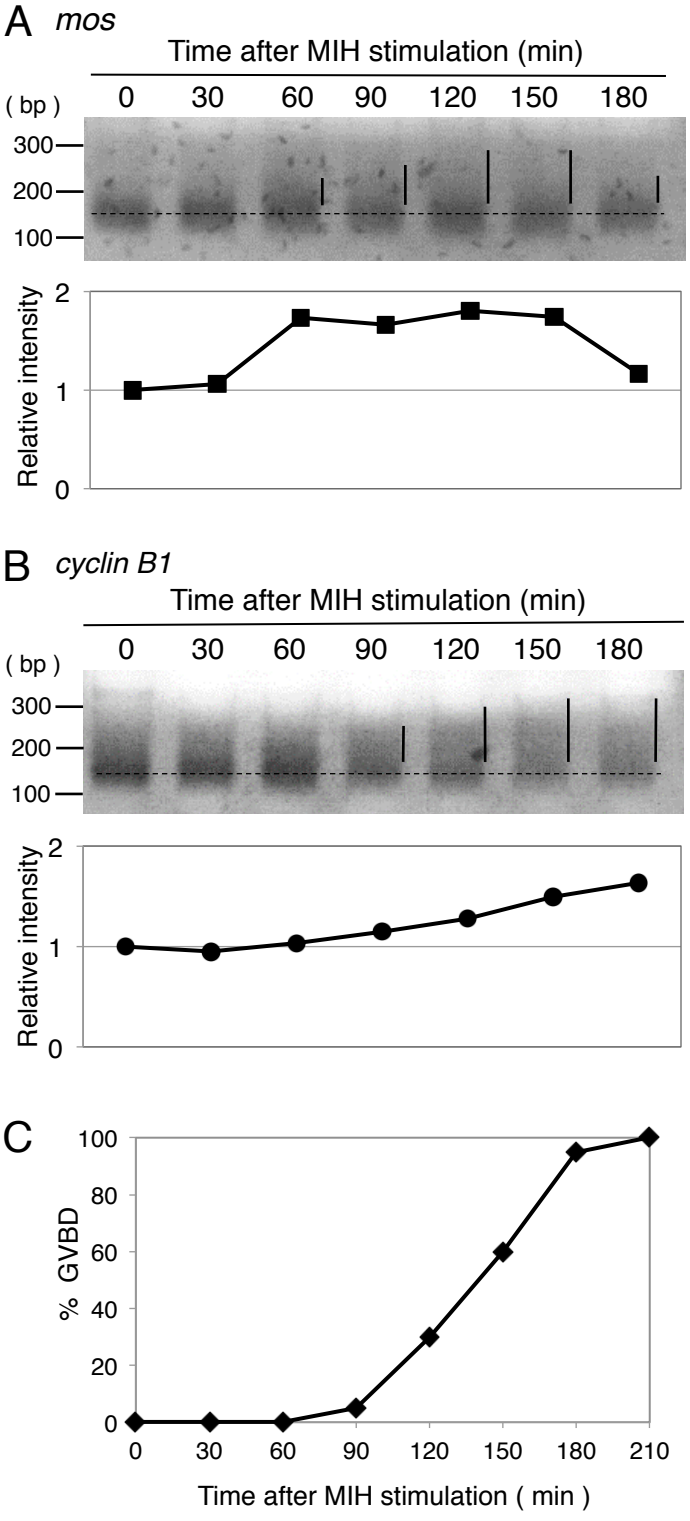
A mos
Time after MIH stimulation (min)
0 30 60 90 120 150 180
(bp)
300
200
100
Relative intensity
2
1
0
B cyclin B1
Time after MIH stimulation (min)
0 30 60 90 120 150 180
(bp)
300
200
100
Relative intensity
2
1
0
C
% GVBD
100
80
60
40
20
0
0 30 60 90 120 150 180 210
Time after MIH stimulation (min)

Fig. 6

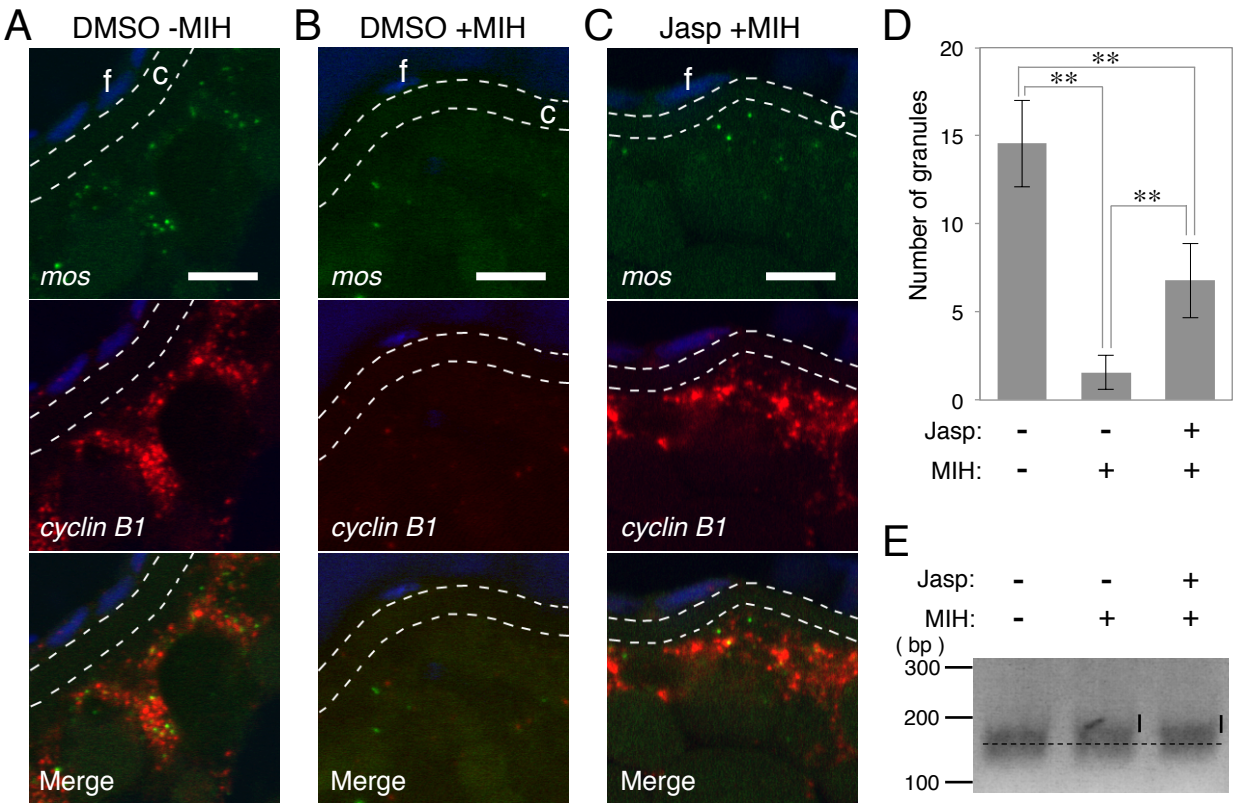
A
DMSO -MIH
B
DMSO +MIH
C
Jasp +MIH
f
c
mos
cyclin B1
Merge
D
Number of granules
20
15
10
5
0
**
**
**
Jasp: - - +
MIH: - + +
E
Jasp: - - +
MIH: - + +
(bp)
300
200
100

Fig. 7